Induction Machine Broken Bar and Stator Short-Circuit Fault Diagnostics Based on Three-Phase Stator Current Envelopes

Aderiano M. da Silva, *Member, IEEE*, Richard J. Povinelli, *Senior Member, IEEE*, and Nabeel A. O. Demerdash, *Fellow, IEEE*

Abstract—A new method for the fault diagnosis of a broken rotor bar and interturn short circuits in induction machines (IMs) is presented. The method is based on the analysis of the three-phase stator current envelopes of IMs using reconstructed phase space transforms. The signatures of each type of fault are created from the three-phase current envelope of each fault. The resulting fault signatures for the new so-called "unseen signals" are classified using Gaussian mixture models and a Bayesian maximum likelihood classifier. The presented method yields a high degree of accuracy in fault identification as evidenced by the given experimental results, which validate this method.

Index Terms—AC motor drive systems, broken bars, envelope detection and classification, fault diagnosis, induction machines (IMs), induction motors, interturn short circuits.

I. INTRODUCTION

INDUCTION machines (IMs) are complex electromechanical devices that are utilized in most industrial applications for the conversion of power from electrical to mechanical form. The IMs can be energized from constant-frequency sinusoidal power supplies or from adjustable-speed ac drives. However, IMs are susceptible to many types of fault, especially when supplied by the ac drives. This is due to the extra voltage stresses on the stator windings, the resulting induced bearing currents, and the high-frequency stator current components caused by such drives. In addition, motor overvoltages can occur because of the length of cable connections between a motor and an ac drive. This last effect is caused by the reflected wave transient voltages [1]. For industrial processes, the IM fault monitoring and diagnosis is important to identify motor failures before they become catastrophic and to prevent severe damage to induction motors. Undetected minor motor faults may cascade into motor failure, which in turn may cause production shutdowns. Such shutdowns are costly in terms of lost production time, maintenance costs, and wasted raw materials.

According to published surveys, IM failures include bearing failures (which are responsible for 40%–50% of all faults), interturn short circuits in stator windings (which represent 30%–40% of the reported faults), and broken rotor bars and end ring faults (which represent 5%–10% of the IM faults) [2]. This paper is centered on electrically detectable faults that occur in the stator windings and rotor cage, namely interturn stator shorts and broken rotor bars.

Significant efforts have been dedicated to the IM fault diagnosis during the last two decades, and many techniques have been proposed [3]–[24]. Several of these fault detection and identification techniques are based on the stator current fast Fourier transform spectral signature analysis, which uses the power spectrum of the stator current [7], [8], [22], [25]. Other techniques include vibration analysis, acoustic noise measurement, torque profile analysis, temperature analysis, and magnetic field analysis [9]–[11], [23]. Recently, new techniques based on artificial intelligence (AI) approaches have been introduced using concepts such as fuzzy logic [12]–[14], [20], [21], [24], genetic algorithms [11], [15], neural network [16], [17], and Bayesian classifiers [18], [26]. Additionally, a method that uses the motor internal physical condition based on a so-called pendulous oscillation of the rotor magnetic field space vector orientation has been introduced for motor fault classification [5], [19].

This paper presents a method that is based on the analysis of the envelope of the three-phase stator current for broken rotor bars and interturn stator shorts. It was found in this investigation that the three-phase current envelope is a powerful feature for motor fault classification. The envelope signal is extracted from the experimentally acquired stator current signals and is used in conjunction with AI techniques based on Gaussian mixture models (GMMs) and reconstructed phase space (RPSs) to identify motor faults. This method creates signatures for each type of fault based on the three-phase stator current envelope. A signature for each newly acquired input set of three-phase stator currents, which are called "unseen signals," must be generated and compared with all the signatures that represent each type of fault learned from the previously acquired database. The conditional likelihoods between this new signature and the previously learned signatures for each type of fault are calculated. Thus, a classifier identifies the previously learned signatures with a maximum likelihood, which now classifies the fault of the so-called "unseen signal" undergoing the process

of classification. In this paper, the classification process yielded high accuracy using just a half second of the current signal for a three-phase 460-V 60-Hz six-pole 5-hp squirrel-cage induction motor, which is roughly the time equivalent of a third of a slip cycle under normal loads. This will be shown and supported by the experimental results presented in Section III. Again, the presented method is focused on two types of motor faults. Specifically, the first type is the broken rotor bar, and the second one is the interturn short circuit in stator windings.

In addition, the presented method not only classifies an IM as healthy or faulty but also identifies the severity of the fault through the identification of the number of broken rotor bars or the number (or percentage) of short-circuited turns in the stator windings. This constitutes a powerful means of monitoring motor fault severities, which could possibly predict the time of onset of the complete failure of a motor and thus could help prevent unexpected shutdowns of industrial processes.

The remainder of this paper is organized as follows: Section II details the method, as well as analyzes and discusses the procedure to obtain the current envelope, and discuses the organization of the data sets. Section III presents the experimental results and analysis for broken bars and interturn short circuits in stator windings. This is followed by an overall discussion of results and conclusions.

II. BACKGROUND

This section presents the induction motor fault diagnosis method and explains the procedure to obtain the three-phase stator current envelope signals for broken rotor bars and interturn short-circuit cases. Additionally, a presentation of the approach taken in organizing the data set is given.

A. Methodology

The fault classification method is based on machine learning techniques [27]. The general concept consists of training the classification algorithm using data sampled from the experimentally acquired three-phase stator currents. These data include different motor operating conditions, including faulty and healthy motor operations. Thus, from each motor operating condition, a signature is generated during the training stage of this method. Additionally, the resulting trained algorithm is tested on the so-called "unseen signals," which constitute the testing set. The accuracy of the motor fault classifier is defined in proportionality to the correctness of the classification of each faulty and healthy case to be identified in the testing set. The training signatures must properly represent the features of each motor operating condition to result in maximum fault diagnosis accuracy.

The process of algorithm training and motor fault classification is based on a previous work detailed in [26], in which one can also find the pseudocode of the approach. In the interest of continuity, essentially, the process consists of constructing a GMM [26] from an RPS [26], [28], [29], where the resulting models are the signatures of the motor operating condition. This RPS-based approach allows for the reconstruction of an IM's state structure [30], [31]. The resulting fault signatures for the "unseen signals" are classified using a Bayesian maximum
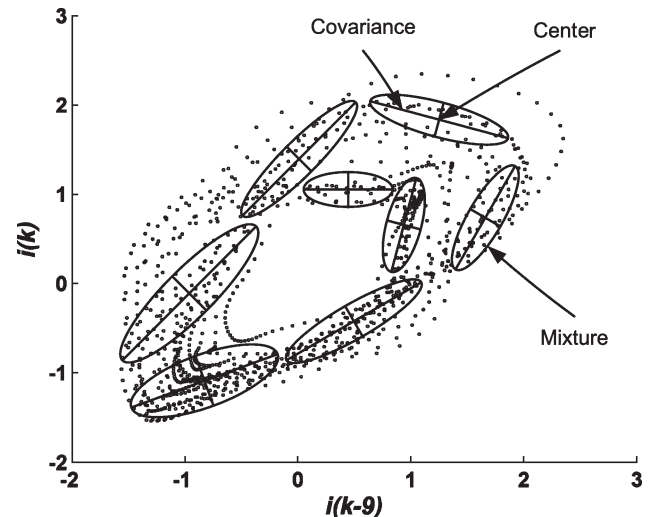

Fig. 1. GMM of the three-phase stator current envelope of a faulty IM RPS with eight mixtures, dimension of 2, and time lag of 9.

likelihood classifier [27]. This process has three steps. The first step is data analysis, where the input signals from the training set are normalized to zero mean and then scaled to unit standard deviation. Moreover, two parameters are calculated to construct the RPS, i.e., the time lag and the dimension. The time lag is calculated using the first minimum of the automutual information function, and the dimension is defined using the global false nearest-neighbor technique [26], [28], [29]. The second step is to learn the GMM of the RPS. The time lag and the dimension are used to build the RPS for each class of motor operating conditions. The GMM is learned with M mixtures for each class of motor operating conditions. The number of mixtures is related to the complexity of the models. A higher number of mixtures implies a more complex model. Ideally, a more complex model provides a higher accuracy in signal classification. However, practically, there is an optimal number of mixtures for maximum accuracy, and past that number, the accuracy tends to be lower. Moreover, the parameters of the GMM (centers and covariances) are estimated by an Expectation Maximization algorithm [26], [32]. A GMM of the RPS with dimension of 2, time lag of 9, and eight mixtures is shown in Fig. 1. Moreover, two parameters of the GMM (centers and covariances) are also shown in Fig. 1. The last step is that of motor fault classification. The signature for an "unseen signal" is classified using the previously trained GMMs. The RPS of the "unseen signal" is constructed with the same dimension and time lag of the previously learned signatures. The Bayesian maximum likelihood classifier [27] computes the conditional likelihood of the signatures for this "unseen signal" under each signature (GMM) previously learned using the training set. The learned signature with maximum likelihood defines the particular class of motor operating condition (faulty or healthy). The algorithm of this overall method is depicted in the functional flow chart of Fig. 2. In this figure, the results obtained in the training stage (a) are followed by the fault classification stage (b) of the algorithm.

The training and testing sets are generated from the envelopes of the three-phase stator current of an induction motor for cases involving healthy and faulty operating conditions,
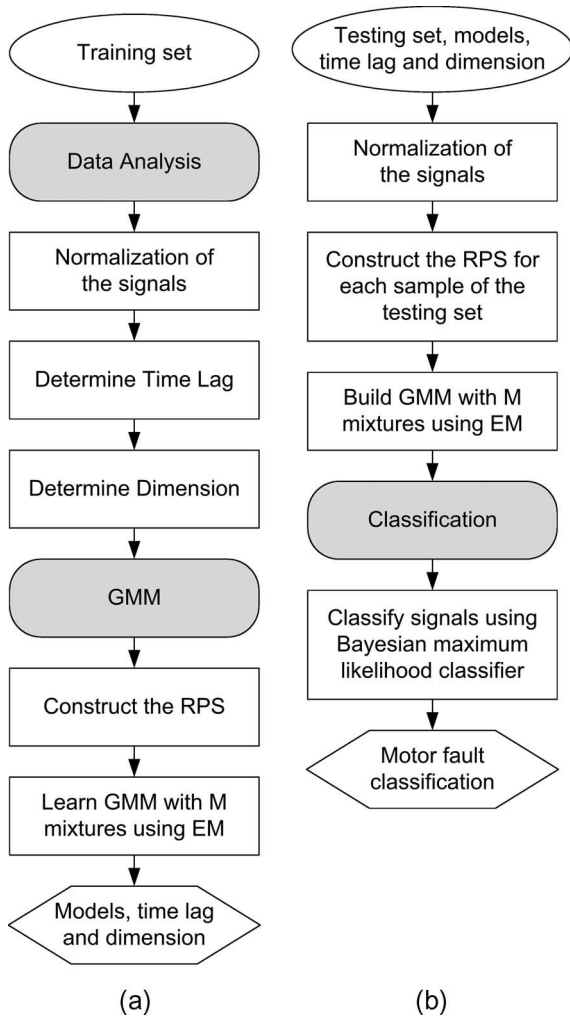
(a)   (b)

Fig. 2.   Algorithm of the presented method. (a) Training stage. (b) Testing or classification stage.
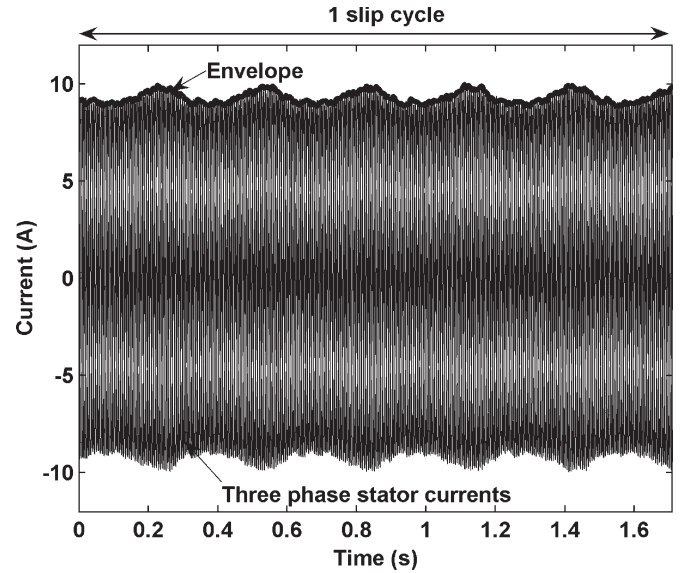

Fig. 3.   One slip cycle of the three-phase stator current envelope for a three-phase 460-V 60-Hz six-pole 5-hp squirrel-cage induction motor with four broken bars under rated load.

Fig. 4.   Laboratory test setup for the 5-hp induction motor and data acquisition.

such as broken rotor bars and interturn short circuits in the stator windings. The training and testing sets are further discussed in the next sections.

B. Three-Phase Stator Current Envelope

The objective of this section is to explain the effect of broken rotor bars and interturn short circuits on the three-phase stator currents of IMs. The broken bars produce a phenomenon called envelope that is cyclically repeated at a rate equal to twice the slip frequency $(2sf)$, and the interturn short circuits cause a profile modification on the three-phase stator current leading to an envelope cyclically repeated at a rate equal to the power frequency (f). The procedure to obtain the three-phase stator current envelope is discussed next.

A healthy rotor has a rotating magnetic field nature that possesses a perfect periodic profile over a two-pole pitch, which leads to a circular trace of the magnetic field's space vector. However, once a rotor develops a single broken bar, the aforementioned periodical profile is lost over the two pole pitches of the rotor containing the broken bar due to the fact that no induced current can flow in the broken bar [5], [19]. Consequently, the magnetic field's neutral plane orientation

deviates from the position for the healthy case, which results in an angular shifting in the rotor magnetomotive force waveform. This angular shifting is a function of the number of broken bars and the geometric distribution of the broken bars around the rotor, and varies with time in a cyclical manner, as explained in [5] and [19]. The distortion of the rotor's magnetic field orientation and the resulting local saturation in the rotor laminations around the region of the broken bars lead to a quasi-elliptical trace of the magnetic field's space vector and consequently modulate in a sequential manner the three-phase stator current. The modulation of the three-phase stator current is the so-called envelope. In this paper, this envelope is the feature used for induction motor fault diagnosis. The envelope resulting from the modulation of the three-phase stator current for a period equivalent to one slip cycle for a faulty 5-hp IM with four broken bars is shown in the experimentally obtained results plotted in Fig. 3. The laboratory test setup used to obtain these data is shown in Fig. 4.
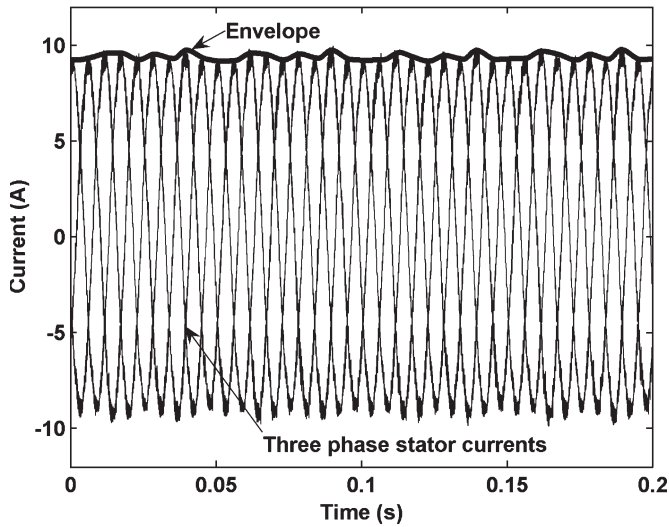
Fig. 5. Three-phase stator current envelope for a three-phase 460-V 60-Hz six-pole 5-hp squirrel-cage induction motor with four interturn short circuits under rated load.
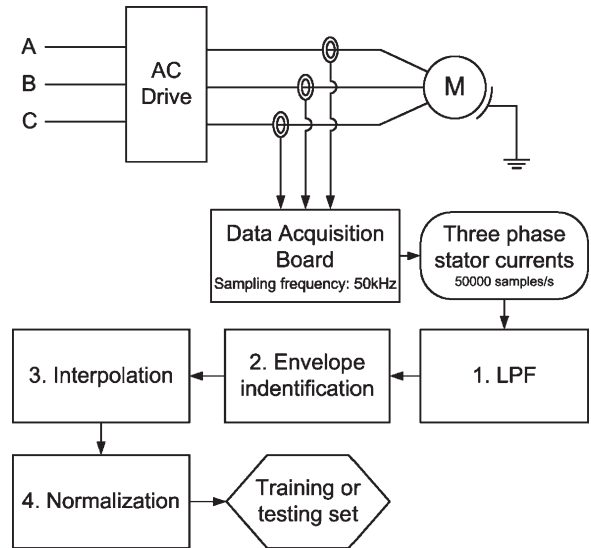

Fig. 6. Procedure to isolate the envelope of the three-phase stator current from an IM supplied by an ac drive for further motor fault classification.

On the other hand, an interturn short circuit principally affects only the stator current of the faulty phase in both profile and peak value. The other stator phase currents suffer smaller interferences. Thus, the stator current profile of each phase is not equally affected by the fault. This three-phase stator current profile modulation is also referred to here as the so-called envelope. Again, the frequency of repetition of this envelope is the power frequency f and not a function of the slip frequency sf, which is associated with broken bar faults. The resulting envelope of the three-phase stator current for the same 5-hp IM with four interturn short circuits without broken bars experimentally obtained under rated load is shown in Fig. 5.

The procedures to obtain the three-phase stator current envelopes for the broken bar and interturn short-circuit cases for learning and classification are identical. This procedure can be summarized in the following steps: 1) low-pass filter (LPF); 2) envelope identification; 3) interpolation; and 4) normalization, see the functional block diagram in Fig. 6. The first step is an LPF, which is essential for the IMs supplied by the ac drives. The stator current of an IM supplied by an ac drive has a high-frequency component due to the carrier frequency responsible for the pulse width modulation (PWM) of the ac drive. Typically, the stator current frequency is variable from 0 to 60 Hz, and the carrier frequency is a fixed value in the range from 4 to 16 kHz. This PWM component is eliminated from the ac current signal by a sixth-order low-pass elliptic digital filter with a cutoff frequency of 2 kHz, a passband of 3 dB, and a stopband of 50 dB [33]. The cutoff frequency was chosen to be 2 kHz because the carrier frequency of the ac drive is at least 4 kHz. Accordingly, the envelope is isolated from the three-phase stator currents without any significant PWM component. The second step, which is envelope identification, consists of extracting from the three-phase currents only the positive peak of each period in each phase. Thus, in 1 s of 60 Hz, the three-phase current signal has 180 positive peaks. In the third step, these few points are interpolated to smoothly represent the dynamic behavior of the three-phase stator current

envelope. The fourth and last step is the z-score normalization that centers the signal at zero mean and scales it to unit standard deviation [34]. After accomplishing these four steps, the identified envelope is used to generate the training set to learn the GMMs or the testing set to classify these unseen input signals with a maximum likelihood Bayes classifier [27]. Again, these steps to isolate the envelope of the three-phase stator currents of a given IM supplied by an ac drive can best be visualized by inspection of Fig. 6. The procedure that utilizes only three current sensors is easily available and implementable in most industrial applications. In most drives, this current information is readily available, and hence, no extra current sensors are needed to implement this procedure (algorithm).

C. Time Series Data Sets

A case-study three-phase 460-V 60-Hz six-pole 5-hp squirrel-cage induction motor supplied by an ac drive operating under scalar (open-loop) constant volts-per-hertz control was tested in the laboratory. This motor has a cage with 45 bars (i.e., 7 1/2 bars per pole pitch), and it has 240 stator winding turns per phase housed in a stator with 36 slots (i.e., six slots per pole and hence two slots per pole per phase). This motor was tested under healthy and one to four broken bars of rotor faulty conditions, as well as one to four interturn shorts in one phase of the stator windings. Thus, this set of tests yielded nine classes of IM operating conditions. An external resistor r_f of 1 Ω was used to emulate a developing or "incipient" interturn short circuit in the stator windings, as depicted in Fig. 7. This resistor also restricts the circulating currents in the shorted portion of the stator winding to a safe level to avoid permanent motor winding damages. In these tests, the loop current in the shorted turn was not allowed to exceed (in root mean square magnitude) three times the rated line current of the motor.

The three-phase stator current was sampled for each class at a 50-kHz sampling frequency using the data acquisition board shown in the functional schematic of Fig. 6. Each class
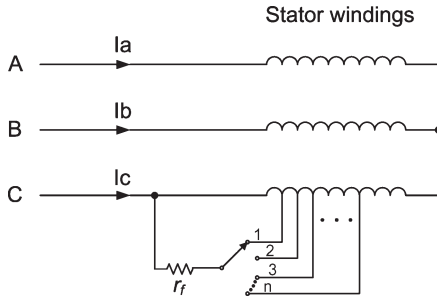
Fig. 7.   Schematic of the tapped induction motor windings.

TABLE I
ACCURACY OF FAULT CLASSIFICATION FOR AN INDUCTION MOTOR WITH
ONE TO FOUR BROKEN BARS AT 60 Hz AND THREE DIFFERENT MOTOR
LOADS BASED ON A TESTING SET WITH 50 SAMPLES

Mixtures	Accuracy (%) (mean ± standard deviation)		
	Motor load as % of Rated Torque		
	50%	75%	100%
4	100±0	100±0	100±0
8	100±0	98±6	100±0
16	100±0	100±0	100±0
32	100±0	100±0	100±0

has 5 s of signal, which results in 250 000 data points each. This 5 s of signal was equally divided into ten samples, where each sample is a time series. The definition of time series is explained in [26]. Thus, the procedure depicted in Fig. 6 was carried out, and the resulting totality of ten time series of each class yielded the training set as well as the testing set using a cross-validation technique [27], [35]. Cross validation is a well-known technique used when the data set is not large enough to obtain totally independent training and testing sets. The cross validation splits the same data set to generate different training and testing sets. The training and test sets were generated by K-fold cross validation with $K = 10$ (see [27] and [35]).

The experiment carried out for broken bars has five classes (one to four broken bars and the healthy case), and for the interturn short circuits, it also has five classes (one to four interturn short circuits and the healthy case). However, the last experiment combines all faults plus the healthy case, thus resulting in nine classes.

Accordingly, the number of samples of the testing set generated using K-fold cross validation is defined by the number of time series per class times the number of classes. These samples of the testing set are distributed in K-folds. Thus, an experiment with five classes ($K = 10$) and ten time series per class has a testing set with 50 samples distributed in ten folds that are to be classified.

III. EXPERIMENTAL VERIFICATION OF THE PRESENTED METHOD

The motor current envelopes obtained from the experimentally acquired motor current data represent two types of motor faults, i.e., broken rotor bars and interturn short circuits in stator windings. The experiment for broken bars was carried out for three different motor loads and for two different ac drive output frequencies, which yields two different motor speeds. On the other hand, the experiment for the interturn short circuits in stator windings was carried out for three values of motor loads at one ac drive output frequency. Finally, the last experiment for broken bars and interturn short circuits yielding nine classes of motor operating conditions was carried out for three levels of motor loads also at one ac drive output frequency. All the experimental results presented below validate the efficacy of this method.

The aforementioned case study of the three-phase 5-hp squirrel-cage induction motor with one to four broken rotor bar faults was tested in the laboratory. The fault classification

results for broken bars with the motor running at 60 Hz and three different levels of loads are shown in Table I. The results for each combination of mixtures of the fault signatures and levels of load torque shown in Table I were generated using a testing set with 50 samples obtained by 10-fold cross-validation. Here, each sample has a duration of 0.5 s of the three-phase stator current envelopes. Accordingly, the one to four broken rotor bars and the healthy motor case yield five classes of motor operating conditions. Again, the motor was tested with three different magnitudes of load that correspond to 50%, 75%, and 100% of the rated torque. It should be pointed out that the rated torque is 30 N·m. As given in Table I, the accuracy of the resulting fault classification for a motor load of 50% and 100% of the rated torque was 100%, i.e., all 50 unseen input samples of the testing set were correctly classified independent of the number of mixtures of the fault signatures. The same level of accuracy was obtained for a motor load of 75% of the rated torque with 4, 16, and 32 fault signature mixtures. However, a slightly lower fault classification accuracy of 98% was obtained and is shown in Table I for the 75% of the rated torque case with eight fault signature mixtures, which means that only one of the 50 samples of the testing set was misclassified. Additionally, the presented fault classification method not only monitors the faults (thus distinguishing a faulty motor from a healthy motor) but also diagnoses the degree of fault severity (thus identifying the number of broken bars). Here, the degree of fault severity is proportional to the number of broken bars. Furthermore, the presented results were carried out for motor loads over 50% of the rated torque. However, the accuracy of the fault classification for motor loads below 50% of the rated torque is slightly lower compared to the accuracies obtained for motor loads above 50% of the rated torque. Below 50% of the rated torque, the amplitude and profile of the envelopes for any number of broken bars become very similar to the healthy case in which the amplitude of the envelope is ideally zero. Thus, when signals with similar envelopes are obtained for a given operating condition under healthy and faulty operations, the implication is that there will be difficulties building sets of signatures that efficiently represent the motor fault operating conditions for accurate motor fault classification. In general, this confirms the well-known fact that it is harder to diagnose a fault when a motor is lightly loaded [36]–[38]. This is an aspect that is further elucidated in Section IV.

Here, Table II presents the accuracy of the broken bar fault classification for the 5-hp motor at rated torque and for two different ac drive output frequencies of 40 and 60 Hz,

TABLE II
ACCURACY OF FAULT CLASSIFICATION FOR AN INDUCTION MOTOR WITH
ONE TO FOUR BROKEN BARS AT 40 AND 60 Hz BASED ON A TESTING SET
WITH 30 SAMPLES. THE TEST WAS CARRIED OUT AT RATED LOAD

Mixtures	Accuracy (%) (mean ± standard deviation)	
	Motor frequency	
	40 Hz	**60 Hz**
4	97±10	100±0
8	97±10	100±0
16	90±16	100±0
32	77±16	100±0

TABLE III
ACCURACY OF FAULT CLASSIFICATION FOR AN INDUCTION MOTOR WITH
ONE TO FOUR INTERTURN SHORT CIRCUITS IN THE STATOR WINDINGS AT
60 Hz AND MOTOR LOADS OF 50%, 75%, AND 100% OF THE RATED
TORQUE BASED ON A TESTING SET WITH 50 SAMPLES

Mixtures	Accuracy (%) (mean ± standard deviation)		
	Motor load as % of Rated Torque		
	50%	**75%**	**100%**
4	94±10	94±10	92±14
8	98±6	96±8	98±6
16	100±0	96±8	98±6
32	100±0	96±8	98±6

TABLE IV
ACCURACY OF FAULT CLASSIFICATION FOR AN INDUCTION MOTOR WITH
ONE TO FOUR BROKEN BARS OR ONE TO FOUR INTERTURN SHORT
CIRCUITS IN STATOR WINDINGS AT 60 Hz AND MOTOR LOADS OF
50%, 75%, AND 100% OF THE RATED TORQUE BASED ON
A TESTING SET WITH 90 SAMPLES

Mixtures	Accuracy (%) (mean ± standard deviation)		
	Motor load as % of Rated Torque		
	50%	**75%**	**100%**
4	91±7	98±5	98±5
8	97±5	98±5	99±4
16	97±5	99±4	99±4
32	99±4	99±4	99±4

respectively. The results for 60 Hz are the same as previously shown in Table I. The testing set for the results at 40 Hz contains 30 samples instead of 50 samples because the original 5 s of the current signals for each class is divided into six samples instead of ten samples, which thus yields the three-phase stator current envelope for each sample with a duration of 0.83 s (5 s/six time series per class). This higher time sample for the 40-Hz data compared to the 60-Hz data is necessary to have samples with approximately the same number of envelope periods for both cases. This time sample of each input signal that is to be classified can be associated with the operating motor frequency in order to automatically adjust the length of the time sample to be used in the classification. One must bear in mind that both the motor frequency and the length of time sample are inversely proportional to each other. An accuracy of 97% was obtained and is shown in Table II at 40 Hz for four and eight fault signature mixtures, which means that this method resulted in only one misclassification out of 30. Table II includes the results with 90% classification accuracy for the 16 fault signature mixtures, which means that this method resulted in three misclassifications out of 30. Meanwhile, an accuracy of 77% for 32 fault signature mixtures was achieved, which means that this method resulted in seven misclassifications for the testing set with 30 samples.

The interturn short circuit is the second type of motor fault investigated in this paper. This type of fault has five classes, i.e., one to four interturn short circuits and a healthy case. The results of accuracy for the classification of the interturn short circuits in the 5-hp motor at 60 Hz and motor loads of 50%, 75%, and 100% of the rated torque are shown in Table III. The motor fault classification is highly accurate with a low standard deviation in all the cases shown in this table. These results were based on a testing set with 50 samples. Thus, a 98% accuracy of classification was achieved, which means that

only one misclassification took place. Meanwhile, the case with 96% classification accuracy represents two misclassifications, and so forth. The different levels of load torque did not result in any loss of accuracy for the classification of interturn short circuits. This lack of effect of load level on the classification results of the shorted turn faults in comparison to the opposite for the cases with broken bars is physically explained in the next section. From Table III, it can be concluded that signatures with 16 mixtures are sufficient to achieve a reasonably high degree of accuracy. However, models with eight mixtures can speed up the learning and classification processes without significant losses in the fault classification accuracy. These fault classification results and associated method constitute a significant contribution for motor fault classification techniques considering that the interturn short circuits represent 30%–40% of the commonly occurring motor faults, with the knowledge that in this method at hand, only the envelopes of the three-phase stator currents are needed.

The last experiment was carried out for one to four broken bars, one to four interturn short circuits, and the healthy motor case, which yield nine classes of operating conditions. Thus, these nine classes yielded a testing set with 90 samples generated by a 10-fold cross-validation method. The results of the accuracy of classification for the nine different motor operating conditions for the aforementioned 5-hp motor at 60 Hz and motor loads of 50%, 75%, and 100% of the rated torque are shown in Table IV. The data in this table also show that a more accurate classification result was obtained for fault signatures with 32 mixtures for any level of motor load over 50% of the rated torque, in which case only one of the 90 samples of the testing set was misclassified, which yields a 99% classification accuracy. These results for 32 fault signature mixtures can be better observed in the so-called "confusion matrix" [35] shown in Table V. The confusion matrix reports the performance of a classifier. It is a square matrix with the dimension defined by the number of classes. The sum of components of each row must contain the same number of samples of the testing set. Each combination of row i and column j contains the number of samples of the testing set classified as the class of the respective column j. A confusion matrix that represents a perfect classifier is a diagonal matrix. Additionally, Table V demonstrates that only one fault was classified as a broken bar fault when it should have been classified as an interturn short circuit. For clarification, it should be pointed out that the headings for the confusion matrix in Table V are defined

TABLE V
CONFUSION MATRIX FOR THE 99% CLASSIFICATION ACCURACY OF THE
INDUCTION MOTOR WITH ONE TO FOUR BROKEN BARS OR ONE TO
FOUR INTERTURN SHORT CIRCUITS IN STATOR WINDINGS AT 60 Hz
AND MOTOR LOADS OF 50%, 75%, AND 100% OF THE RATED
TORQUE BASED ON A TESTING SET OF 90 SAMPLES AND
WITH 32 FAULT SIGNATURE MIXTURES

		Classified faults								
		1B	2B	3B	4B	H	S1	S2	S3	S4
Real faults	1B	10	0	0	0	0	0	0	0	0
	2B	0	10	0	0	0	0	0	0	0
	3B	0	0	10	0	0	0	0	0	0
	4B	0	0	0	10	0	0	0	0	0
	H	0	0	0	0	10	0	0	0	0
	S1	1	0	0	0	0	9	0	0	0
	S2	0	0	0	0	0	0	10	0	0
	S3	0	0	0	0	0	0	0	10	0
	S4	0	0	0	0	0	0	0	0	10

as follows: 1B ≡ one broken bar, 2B ≡ two broken bars, 3B ≡ three broken bars, 4B ≡ four broken bars, H ≡ healthy, S1 ≡ one turn short circuited, S2 ≡ two turns short circuited, S3 ≡ three turns short circuited, and S4 ≡ four turns short circuited. These results demonstrate the relatively high degree of accuracy of fault classification that is associated with the use of the method subject of this paper.

IV. DISCUSSION OF RESULTS

In this paper, a 5-hp induction motor was investigated for the monitoring and diagnosis of broken rotor bars and interturn short circuits in stator windings with three different magnitudes of motor loads. The three-phase stator current envelope was found here to be a powerful feature of the induction motor for fault classification. Each healthy and faulty motor operating condition yielded a signature generated from the three-phase stator current envelope using the GMMs of RPS. The conditional probability of a fault signature for any "unseen signal" was computed for each given signature previously generated during the training stage. Thus, this "unseen signal" was classified using the Bayesian maximum likelihood classifier.

The three-phase stator current envelope for broken bar faults depends on the number and geometric distribution of the broken bars. Two motors with identical ratings and with the same number of broken bars but with different geometrical distributions of the broken rotor bars may yield a misclassification of this fault, because the signatures are learned for a specific number and distribution of broken bars. Different distributions for the same number of broken bars may yield different signatures. Thus, a signature learned for a specific number and distribution of broken bars cannot guarantee a correct classification of the same number of broken bars for different geometrical distributions. This is an open problem not only for the method presented in this paper but also for other techniques that analyze the stator currents [5], [7].

The presented method is exclusively based on the analysis of the three-phase stator current envelopes. The inputs of the presented method are only the training and testing sets composed from experimentally obtained samples of the three-phase stator current envelopes for different motor operating conditions. Thus, there is no need for any other information about the

induction motor or its various parameters during the training and testing stages. Moreover, mathematical models of the IMs, ac drives, or any other mathematical formulation or knowledge about the IM are not required. This simplifies the motor fault classification problem because complex calculations related to IMs as well as any specific design information about each individual motor for the purposes of fault diagnostics are not involved. However, the presented method at this point needs signatures built for each different fault at different speeds and torques. This yields many signatures to represent the range of all the possible motor operating conditions. Therefore, the number of signatures may be reduced if the signatures built for a specific operating condition, for example, rated speed and torque, are scaled for any other different operating condition. In this case, the signature generated for the rated conditions must be associated with speed and torque in order to scale it for use in any other motor operating condition. The speed can be directly obtained from either the ac drive, a speed sensor, or a sensorless speed estimator. The torque can be either measured by a torque transducer or calculated through a sensorless torque estimator. Thus, the signatures can be automatically redefined for any value of speed and torque of an IM.

The presented method yielded a high degree of accuracy of motor fault classification even with the IM running at different levels of load torque. This statement is best validated in Table IV, which presents the accuracies of fault classification for nine different healthy and faulty cases of the 5-hp IM. Moreover, Table IV shows the accuracy of motor fault classification for three different levels of load torque and four different numbers of fault signature mixtures. Here, the number of mixtures is manually defined through the analysis of the classification results. From an investigation of Table IV, it can be concluded that the best number of fault signature mixtures is 32 because the accuracy remains high at 99% for any level of motor load. However, the speed of the training and testing stages of the presented method is directly related to the number of fault signature mixtures. Thus, the presented method can always be speeded up (hastened) in real time by using less fault signature mixtures. From further examination of Table IV, it can be concluded that an accuracy of over 97% was obtained with the eight fault signature mixtures for any level of motor load over 50% of the rated load, which is deemed reasonable for general industrial applications. In this case, eight mixtures satisfy the requirement for both a reasonable level of fault classification accuracy and required time of the training and testing processes.

The well-known difficulties normally associated with diagnosing motor faults at light loads [36]–[38] were also encountered here. It is observed that the accuracy of this diagnostic method deteriorated for motor loads under 50% of the rated load values. This is not a new difficulty, and other methods documented in the literature suffer from similar difficulties [36]–[38]. This can be physically attributed to the fact that under light load, the rotor electric circuit approaches the high-impedance no-load condition, in which the effect of any change in the cage impedance can be masked due to its weak impact at the stator terminals. Furthermore, from a magnetic field point of view, at rated or near rated load, the currents in the bars of

a squirrel cage act as a magnetic shield to the bulk of the rotor iron core, and hence that core remains relatively unsaturated or lightly saturated with a good degree of magnetic circular symmetry (no saliency effects). When bar breakages do occur at rated or near rated load conditions, the magnetic shielding effect of the bars is lost at the location of such bar breakage with a resulting higher degree of local magnetic saturation appearing at that spot. Hence, the rotor's circular magnetic symmetry is lost, and an "apparent magnetic saliency or asymmetry" appears in the rotor. This asymmetry rotates at slip speed with respect to the synchronously rotating magnetic field, and this interturn gives rise to the envelope appearing to enclose the three-phase current waveforms. Hence, it is easier to diagnose such a fault using such an envelope under such substantial motor loads. The phenomenon exploited here in this method is muted or weak at light loads and hence arises the difficulty in diagnosis below 50% of rated load for the 5-hp case study of this paper.

Although a short circuit between turns of two phases and a short circuit in turns of all the phases due to overload or blocked rotor are possible, an interturn short circuit generally first occurs in just one phase. In this case, the stator current envelope of each single phase is not equally modulated. The stator current envelope of the healthy phases is slightly affected by the faulty phase, while the envelope of the faulty phase is highly modulated. Here, an analysis of the stator current envelope of only one phase instead of the three phases cannot be sufficient to correctly diagnose a faulty condition, particularly if this analyzed phase is not the faulty phase. This addresses the reason for the use of a three-phase stator current envelope instead of a single-phase stator current envelope. Independent of the phase in which turns are short circuited, the three-phase stator current envelope associated with the method presented in this paper is sufficient to classify interturn short-circuit faults. It should be pointed out that difficulties were not encountered in the diagnosis of shorted stator turns at light loads because the fault is exclusively a stator circuit phenomenon, which is detectable independent of the level of load that as mentioned above largely affects the circuit of the rotor.

Additionally, the three-phase stator current envelope constitutes an IM feature that is associated with the method subject of this paper and not only helps monitor a healthy and faulty condition but also diagnoses the number of interturn short circuits in stator windings or the number of broken rotor bars. This diagnostic method yields further important information about the motor operating condition, namely the fault severity. Here, the fault severity is directly related to the number of broken bars or the number of turns involved in an interturn short circuit.

V. CONCLUSION AND FUTURE WORK

This paper has presented a motor fault diagnosis method for IMs based on three-phase stator current envelopes for broken rotor bars and interturn short circuits in stator windings. Motor fault signatures were generated using GMMs of the RPS transforms. The maximum likelihood of the signature generated for an unseen acquired signal under the previously learned signatures defines the fault class using the Bayesian maximum likelihood classifier.

The high degree of accuracy evidenced through the results suggests that the proposed method can constitute a powerful tool for induction motor fault diagnosis. Moreover, this method not only monitors the IM identifying whether the motor is healthy or faulty but also diagnoses the severity of the fault, i.e., identifying the number of broken bars or the number of turns involved in one interturn short circuit. This characteristic is very import to prevent irreversible motor damages and unexpected shutdown of industrial processes, and to reduce the downtime and cost of production processes.

Future works will use independent training and testing sets. The training set, in addition to containing actual experimentally obtained results, may be augmented by healthy and faulty motor performance data generated by commercial finite-elements software (Magsoft) based on finite-element methods, while the testing set would be exclusively acquired from an experimental setup or field-acquired data. This would allow the enlargement of the nature of classes of faults to be analyzed and diagnosed.

REFERENCES

[1] D. Leggate, J. Pankau, D. Schlegel, R. Kerkman, and G. Skibinski, "Reflected waves and their associated current," in *Conf. Rec. 33rd IAS Annu. Meeting*, 1998, pp. 789–798.

[2] S. Nandi and H. A. Toliyat, "Condition monitoring and fault diagnosis of electrical machines—A review," in *Conf. Rec. 34th IAS Annu. Meeting*, 1999, pp. 197–204.

[3] J. Penman, H. G. Sedding, B. A. Lloyd, and W. T. Fink, "Detection and location of interturn short circuits in the stator windings of operating motors," *IEEE Trans. Energy Convers.*, vol. 9, no. 4, pp. 652–658, Dec. 1994.

[4] C. J. Dister and R. Schiferl, "Using temperature, voltage, and/or speed measurements to improve trending of induction motor RMS currents in process control and diagnostics," in *Conf. Rec. 33rd IAS Annu. Meeting*, 1998, pp. 312–318.

[5] B. Mirafzal and N. A. O. Demerdash, "Induction machine broken-bar fault diagnosis using the rotor magnetic field space-vector orientation," *IEEE Trans. Ind. Appl.*, vol. 40, no. 2, pp. 534–542, Mar./Apr. 2004.

[6] M. E. H. Benbouzid, "Bibliography on induction motors faults detection and diagnosis," *IEEE Trans. Energy Convers.*, vol. 14, no. 4, pp. 1065–1074, Dec. 1999.

[7] M. E. H. Benbouzid, "A review of induction motors signature analysis as a medium for faults detection," *IEEE Trans. Ind. Electron.*, vol. 47, no. 5, pp. 984–993, Oct. 2000.

[8] G. B. Kliman, R. A. Koegl, J. Stein, R. D. Endicott, and M. W. Madden, "Noninvasive detection of broken rotor bars in operating induction motors," *IEEE Trans. Energy Convers.*, vol. 3, no. 4, pp. 873–879, Dec. 1988.

[9] D. G. Dorrell, W. T. Thomson, and S. Roach, "Analysis of airgap flux, current, and vibration signals as a function of the combination of static and dynamic airgap eccentricity in 3-phase induction motors," *IEEE Trans. Ind. Appl.*, vol. 33, no. 1, pp. 24–34, Jan./Feb. 1997.

[10] S. Fruchtenicht, E. Pittius, and H. O. Seinsch, "A diagnostic system for three-phase asynchronous machines," in *Proc. 4th Int. Conf. Elect. Mach. Drives*, 1989, pp. 163–171.

[11] A. Siddique, G. S. Yadava, and B. Singh, "A review of stator fault monitoring techniques of induction motors," *IEEE Trans. Energy Convers.*, vol. 20, no. 1, pp. 106–114, Mar. 2005.

[12] F. Zidani, M. E. H. Benbouzid, D. Diallo, and M. S. Nait-Said, "Induction motor stator faults diagnosis by a current Concordia pattern-based fuzzy decision system," *IEEE Trans. Energy Convers.*, vol. 18, no. 4, pp. 469–475, Dec. 2003.

[13] M. E. H. Benbouzid and H. Nejjari, "A simple fuzzy logic approach for induction motors stator condition monitoring," in *Proc. IEEE Int. Elect. Mach. Drives Conf.*, 2001, pp. 634–639.

[14] I. Lasurt, A. F. Stronach, and J. Penman, "A fuzzy logic approach to the interpretation of higher order spectra applied to fault diagnosis in electrical machines," in *Proc. 19th Int. Conf. North Amer. Fuzzy Inf. Process. Soc.*, 2000, pp. 158–162.

[15] L. Cristaldi, M. Lazzaroni, A. Monti, F. Ponci, and F. E. Zocchi, "A genetic algorithm for fault identification in electrical drives: A comparison with neuro-fuzzy computation," in *Proc. 21st IEEE IMTC*, 2004, pp. 1454–1459.

[16] F. Filippetti, G. Franceschini, and C. Tassoni, "Neural networks aided online diagnostics of induction motor rotor faults," in *Conf. Rec. IAS Annu. Meeting*, 1993, pp. 316–323.

[17] M. Chow and S. O. Yee, "Methodology for on-line incipient fault detection in single-phase squirrel-cage induction motors using artificial neural networks," *IEEE Trans. Energy Convers.*, vol. 6, no. 3, pp. 536–545, Sep. 1991.

[18] M. Haji and H. A. Toliyat, "Pattern recognition—A technique for induction machines rotor broken bar detection," *IEEE Trans. Energy Convers.*, vol. 16, no. 4, pp. 312–317, Dec. 2001.

[19] B. Mirafzal and N. A. O. Demerdash, "Effects of load magnitude on diagnosing broken bar faults in induction motors using the pendulous oscillation of the rotor magnetic field orientation," *IEEE Trans. Ind. Appl.*, vol. 41, no. 3, pp. 771–783, Jun. 2005.

[20] B. Ayhan, M.-Y. Chow, and M.-H. Song, "Multiple discriminant analysis and neural-network-based monolith and partition fault-detection schemes for broken rotor bar in induction motors," *IEEE Trans. Ind. Electron.*, vol. 53, no. 4, pp. 1298–1308, Jun. 2006.

[21] M. S. Ballal, Z. J. Khan, H. M. Suryawanshi, and R. L. Sonolikar, "Adaptive neural fuzzy inference system for the detection of inter-turn insulation and bearing wear faults in induction motor," *IEEE Trans. Ind. Electron.*, vol. 54, no. 1, pp. 250–258, Feb. 2007.

[22] J.-H. Jung, J.-J. Lee, and B.-H. Kwon, "Online diagnosis of induction motors using MCSA," *IEEE Trans. Ind. Electron.*, vol. 53, no. 6, pp. 1842–1852, Dec. 2006.

[23] H. Su and K. T. Chong, "Induction machine condition monitoring using neural network modeling," *IEEE Trans. Ind. Electron.*, vol. 54, no. 1, pp. 241–249, Feb. 2007.

[24] W. W. Tan and H. Huo, "A generic neurofuzzy model-based approach for detecting faults in induction motors," *IEEE Trans. Ind. Electron.*, vol. 52, no. 5, pp. 1420–1427, Oct. 2005.

[25] A. Bellini, F. Filippetti, G. Franceschini, C. Tassoni, and G. B. Kliman, "Quantitative evaluation of induction motor broken bars by means of electrical signature analysis," *IEEE Trans. Ind. Appl.*, vol. 37, no. 5, pp. 1248–1255, Sep./Oct. 2001.

[26] R. J. Povinelli, M. T. Johnson, A. C. Lindgren, and J. Ye, "Time series classification using Gaussian mixture models of reconstructed phase spaces," *IEEE Trans. Knowl. Data Eng.*, vol. 16, no. 6, pp. 779–783, Jun. 2004.

[27] T. M. Mitchell, *Machine Learning*. New York: McGraw-Hill, 1997.

[28] H. D. I. Abarbanel, *Analysis of Observed Chaotic Data*. New York: Springer-Verlag, 1996.

[29] H. Kantz and T. Schreiber, *Nonlinear Time Series Analysis*, 2nd ed. Cambridge, U.K.: Cambrige Univ. Press, 2004.

[30] T. Sauer, J. A. Yorke, and M. Casdagli, "Embedology," *J. Stat. Phys.*, vol. 65, no. 3/4, pp. 579–616, Nov. 1991.

[31] F. Takens, "Detecting strange attractors in turbulence," in *Proc. Dynamical Syst. Turbulence*, 1980, pp. 366–381.

[32] T. K. Moon, "The expectation-maximization algorithm," *IEEE Signal Process. Mag.*, vol. 13, no. 6, pp. 47–60, Nov. 1996.

[33] A. V. Oppenheim and R. W. Schafer, *Discrete-Time Signal Processing*, 2nd ed. Englewood Cliffs, NJ: Prentice-Hall, 1999.

[34] R. O. Duda, P. E. Hart, and D. G. Stork, *Pattern Classification*, 2nd ed. New York: Wiley-Interscience, 2000.

[35] S. M. Weiss and C. A. Kulikowski, *Computer Systems That Learn: Classification and Prediction Methods from Statistics, Neural Nets, Machine Learning, and Expert Systems*. San Mateo, CA: Morgan Kaufmann, 1991.

[36] W. T. Thomson and M. Fenger, "Industrial application of current signature analysis to diagnose faults in 3-phase squirrel cage induction motors," in *Proc. Conf. Rec. Annu. Pulp Paper Ind. Tech. Conf.*, 2000, pp. 205–211.

[37] A. M. Trzynadlowski and E. Ritchie, "Comparative investigation of diagnostic media for induction motors: A case of rotor cage faults," *IEEE Trans. Ind. Electron.*, vol. 47, no. 5, pp. 1092–1099, Oct. 2000.

[38] S. M. A. Cruz and A. J. M. Cardoso, "Rotor cage fault diagnosis in three-phase induction motors by the total instantaneous power spectral analysis," in *Conf. Rec. 34th IAS Annu. Meeting*, 1999, pp. 1929–1934.

Aderiano M. da Silva (S'05–M'06) received the B.S. degree in control and automation engineering from the Pontifical Catholic University of Rio Grande do Sul, Porto Alegre, Brazil, in 2004 and the M.S. degree in electrical engineering from Marquette University, Milwaukee, WI, in 2006.

From 1999 to 2003, he was an Industrial Automation and Controls Designer with the largest manufacturing of road equipments in South America. From 2004 to 2006, he was a Research Assistant with the Department of Electrical and Computer Engineering, Marquette University. Since 2006, he has been a Technical Consultant with Rockwell Automation, Mequon, WI. His research interests include fault diagnostics of electric machines and drive, as well as AI techniques, robotics, and control system stability and performance.

Richard J. Povinelli (S'85–M'97–SM'01) received the B.S. degree in electrical engineering and the B.A. degree in psychology in 1987 from the University of Illinois, Champaign-Urbana, the M.S. degree in computer and systems engineering from Rensselaer Polytechnic Institute, Troy, NY, in 1989, and the Ph.D. degree in electrical and computer engineering from Marquette University, Milwaukee, WI, in 1999.

From 1987 to 1990, he was a Software Engineer with the General Electric Corporate Research and Development. From 1990 to 1994, he was with GE Medical Systems, where he served as Program Manager and then as Global Project Leader. From 1995 to 1998, he was a Lecturer and an Adjunct Assistant Professor with the Department of Electrical and Computer Engineering, Marquette University, where he has been an Assistant Professor since 1999. His research interests include data mining of time series, chaos and dynamical systems, computational intelligence, and financial engineering.

Dr. Povinelli is a Senior Member of the Association for Computing Machinery, American Society of Engineering Education, Tau Beta Pi, Phi Beta Kappa, Sigma Xi, Eta Kappa Nu, Upsilon Pi Epsilon, and Golden Key. He was voted the Young Engineer of the Year for 2003 by the Engineers and Scientists of Milwaukee, Inc.

Nabeel A. O. Demerdash (M'65–SM'74–F'90) received the B.Sc.E.E. degree (distinction with first class honors) from Cairo University, Cairo, Egypt, in 1964, and the M.S.E.E. and Ph.D. degrees from the University of Pittsburgh, Pittsburgh, PA, in 1967 and 1971, respectively.

From 1968 to 1972, he was a Development Engineer with the Large Rotating Apparatus Development Engineering Department, Westinghouse Electric Corporation, East Pittsburgh, PA. From 1972 to 1983, he was an Assistant Professor, Associate Professor, and Professor with the Department of Electrical Engineering, Virginia Polytechnic Institute and State University, Blacksburg. From 1983 to 1994, he was a Professor with the Department of Electrical and Computer Engineering, Clarkson University, Potsdam, NY. Since 1994, he has been a Professor with the Department of Electrical and Computer Engineering, Marquette University, Milwaukee, WI, where he served as Department Chair from 1994 to 1997. He is the author or coauthor of more than 100 papers published in various IEEE TRANSACTIONS. His research interests include power electronic applications to electric machines and drives, electromechanical propulsion and actuation, computational electromagnetics in machines and drives, and diagnostics and modeling of harmonic effects on machine power systems dynamics.

Prof. Demerdash is a member of the American Society of Engineering Education, Sigma Xi, and the Electromagnetics Academy. He is active in the Electric Machinery Committees of the IEEE Power Engineering Society (PES) and its various subcommittees, as well as the Electric Machines Committee of the IEEE Industry Applications Society. He is listed in the Distinguished Lecturer Program of the PES and the Distinguished Speaker Program of the IEEE Industrial Electronics Society. He was the recipient of the 1999 IEEE Nikola Tesla Technical Field Award. He is also the recipient of two 1993 Prize Paper Awards from both the PES and its Electric Machinery Committee, and two 1994 Working Group Awards from both the PES and its Electric Machinery Committee.